Journal of Food Engineering 340 (2023) 111309

Contents lists available at ScienceDirect

Journal of Food Engineering

journal homepage: www.elsevier.com/locate/jfoodeng

Generalized moisture diffusivity for food drying through multiscale modeling

Zachary G. Welsh [a], Matthew J. Simpson [b], Md Imran H. Khan [a], M.A. Karim [a,*]

[a] School of Mechanical, Medical and Process Engineering, Queensland University of Technology, Brisbane, Australia
[b] School of Mathematical Sciences, Queensland University of Technology, Brisbane, Australia

ARTICLE INFO

Keywords:
Generalized diffusivity
Multiscale modeling
Cell rupturing
Food drying

ABSTRACT

Drying plant-based food materials can be time consuming and energy intensive, making optimization of its processes essential. However, current mathematical models are plagued with condition-dependent diffusivities restricting their performance in developing optimal drying strategies. Multiscale modeling is one technique which can help transition towards a more physics-based approach, improving model's predictive capabilities. This research constructs a multiscale food drying model utilizing a generalized moisture diffusivity to investigate its predictive capabilities. The study investigates two food materials (apple and potato) convective drying at two different temperatures (47 °C and 64 °C). Additionally, to be able to utilize the generalized diffusivity, cell rupturing must be considered. Therefore, a theoretical rupturing threshold was developed exploiting the equilibrium vapor pressure to recognize which transport mechanisms were occurring. The generalized diffusivity was able to distinguish between the two materials and was able to describe the experimental data accurately at both drying temperatures. The generalized property resulted in diffusivities with the range of 1.94×10^{-10}-5.14×10^{-10} m^2/s.

1. Introduction

Drying plant-based food materials, such as fruits and vegetables, involves simultaneous heat and mass transport with anisotropic deformation (Mahiuddin et al., 2018). Drying can be very time consuming and energy intensive making optimization of its processes, systems and configurations very important. Mathematical modeling is crucial in the development of optimal drying strategies, since a modeling and simulation-based approach facilitates the investigation of multiple design and control configurations for a wide range of process conditions (Defraeye, 2014). However, current mathematical food drying models are plagued with condition-dependent properties with limited predictive capabilities, restricting a model's performance in these optimization scenarios. Transitioning to a detailed physics-based model which incorporates additional physics will help in improving a model's predictive capabilities while reducing its reliance on empirical information.

Multiscale modeling can help transition towards a more physics-based approach. Multiscale modeling is considered to be a series of sub-models which investigates the behavior, such as moisture migration, of a particular product over multiple spatial scales, considering substantial physics for a reasonable computational cost (Welsh et al., 2018). One property which can greatly benefit from multiscale modeling is the diffusivity of moisture.

Considering condition-dependent moisture diffusivity has been very common in mathematical food drying models. This has been a forced preference, due to the lack of comprehensive knowledge of the transport phenomena occurring, complex deformation and heterogeneous structure of the material (Welsh et al., 2018; Adrover et al., 2019). Commonly, to model moisture migration, all transport mechanisms are lumped and Fickian diffusion is assumed. The effective diffusivity is then estimated through curve fitting techniques and the Arrhenius framework. These curve fitting techniques are high in experimental cost and often consider a perfect geometry with no deformation, causing the predictive model and experimental data to significantly deviate in the latter stage of drying (Tzempelikos et al., 2015). In reality, the moisture transport depends on many interacting processes and is strongly influenced by deformation. The migration of intracellular water (ICW) also plays a major role as it can cause dynamic modifications to the materials structure (uneven volume reductions and cell rupturing). Due to its influence, many researchers have attempted to incorporate deformation within their models (Mahiuddin et al., 2018). Adrover et al. (2019) considered a moving boundary model for isothermal drying and

* Corresponding author. Queensland University of Technology2 George Street, QLD, 4000, Australia.
E-mail address: azharul.karim@qut.edu.au (M.A. Karim).

https://doi.org/10.1016/j.jfoodeng.2022.111309
Received 19 July 2022; Received in revised form 25 September 2022; Accepted 29 September 2022
Available online 8 October 2022

shrinkage of food material. The work accounted for the volume reduction, borrowing literature from the swelling of polymer matrices, and investigated two approaches to diffusivity, a constant diffusivity and a diffusivity in terms of the volume reduction. With recent advances in cellular experimental investigating techniques (Khan et al., 2018), models have been transitioning towards more mechanistic approaches. Dadmohammadi and Datta (2019) introduced a new diffusivity function, using a more mechanistic approach. The approach treats the material as a porous media, using parameters such as relative permeability, porosity, tortuosity and constrictivity. However, the approach still only models the macroscale requiring unique phase dependent diffusivities for each material. Qiu et al. (2022) constructed a more mechanistic model for impingement drying of a porous slab, utilizing fractal scaling laws and porous media concepts. Their work considered the material's pore structure for the effective gas and vapor diffusivity coefficients, however, relied on a macroscale condition dependent diffusivity for water and failed to consider ICW. Prawiranto et al. (2020) conducted an in-silico investigation of how the microstructural changes in fruit affected the drying kinetics of a material. The work utilized X-ray micro-computed tomography images to consider the material's structure and conducted a comprehensive parametric study on possible microstructural changes which could occur. However, the work did not predict which cellular deformation would occur due to the macroscale/drying conditions and only investigated one material drying at a low temperature (23 °C) under no external heat source. Welsh et al. (2021a) developed a food drying model considering multiscale strategies for drying apple. The work utilized average diffusivities with predetermined temperature dependent microscales, requiring extensive experimental data. However, to utilize the full predictive capabilities of multiscale modeling, the microscale model should be dynamic and coupled to the processes occurring at a macroscale. The deformation of food material under an external heat source, especially the presence of cell rupturing, adds complexity to achieving this goal. Welsh et al. (2021b) further extended the multiscale modeling approach by conducting a temporal investigation on drying apples at 60 °C. By varying the microscale domain and utilizing extensive experimental data, they were able to consider the effects of cell rupturing within the microscale domains while inversely calculating the cellular diffusivity of ICW. However, though the development of the cellular property overcame some limitations of their previous work (specifically the need for an average diffusivity and predetermined temperature dependent domains), the work only investigated drying at 60 °C, drying one material (apples) and did not incorporate cell rupturing within the macroscale of the multiscale physics-based model.

Based on these preliminary works, we proposed an advanced multiscale food drying model, capable of incorporating cell rupturing and modeling different materials, to investigate the full predictive capabilities of multiscale modeling. The work investigates two different food materials (apple and potato) convective drying at two different temperatures (47 °C and 64 °C). The model develops a single upscaled effective diffusivity for all food materials. Additionally, to be able to utilize the upscaled property, cell rupturing must be practically considered. Therefore, a cell rupturing investigation is conducted to develop a theoretical threshold in order to characterize which transport mechanisms are occurring. The results are validated and compared to experimental data.

2. Model development

2.1. Drying model

The core multiscale model was developed previously (Welsh et al., 2021a) considering two spatial scales, a microscale scale and a macroscale, Fig. 1. The definition/classification of these scales is arbitrary and their naming is often quite product or field/industry specific (Defraeye, 2014), i.e. the microscale can also be referred to as a mesoscale

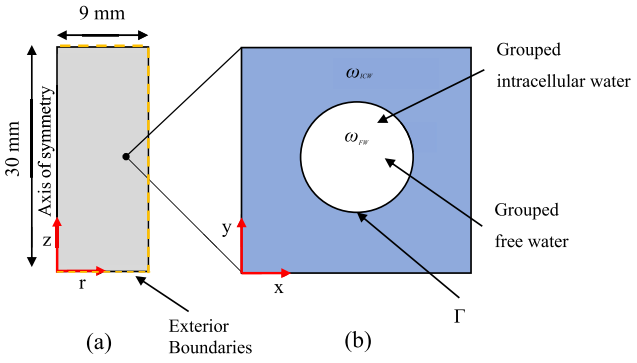

Fig. 1. Domains (a) axisymmetric macroscale domain and (b) microscale domain.

depending on the field and the macroscale can also be called the dryer or tissue scale. To be consistent with previously published literature (Welsh et al., 2021a, 2021b; Perré, 2007), the fine scale (cellular structure) is defined as the microscale and the coarse scale (tissue level) is defined as the macroscale. This study extends the model, introducing the novel rupture threshold while investigating the generalized diffusivity. The macroscale transport model was developed using an axisymmetric coordinate system, Fig. 1 (a), based on the following assumptions: (1) internal convective flow and heat generation can be neglected, (2) drying air properties are constant, (3) axisymmetric heating occurs, (4) moisture is only evaporated from the surface and (5) thermal equilibrium exists between all phases. Due to computational cost and limitation in current deformation models, the macroscale deformation was not considered (Mahiuddin et al., 2018).

2.2. Macroscale conservation equations

The macroscale conservation equations for mass and energy are based on Fick's law of diffusion and Fourier's law of heat transfer. These equations solve for the moisture concentration C (mol/m^3) and temperature T (K) in terms of position and time. The respective equations are given by

$$\frac{\partial C}{\partial t}+\frac{1}{r}\frac{\partial}{\partial r}\left[-D_{H,eff}\,r\,\frac{\partial C}{\partial r}\right]+\frac{\partial}{\partial z}\left[-D_{H,eff}\frac{\partial C}{\partial z}\right]=0 \quad , \tag{1}$$

$$\rho c_p\frac{\partial T}{\partial t}+\frac{1}{r}\frac{\partial}{\partial r}\left[-k\,r\,\frac{\partial T}{\partial r}\right]+\frac{\partial}{\partial z}\left[-k\frac{\partial T}{\partial z}\right]=0 \quad , \tag{2}$$

where t is the time (s), ρ is the density of the food tissue (kg/m^3), c_p is the specific heat of the food tissue (J/(kg·K)) k is the thermal conductivity of the food material (W/(m·K)) and $D_{H,eff}$ is the upscaled effective moisture diffusivity (m^2/s). The effective moisture diffusivity depends on the temperature at any given point within the sample and WC_{ICW}, the ICW content (%).

2.3. Macroscale boundary conditions

The boundary conditions for the mass flux and heat transfer at the exterior surface was given by,

$$\mathbf{n}\cdot\left[-D_{H,eff}\nabla C\right]=h_m\frac{\left(p_{v\ eq}-p_{v\ air}\right)}{RT} \quad , \tag{3}$$

$$\mathbf{n}\cdot\left[-k\nabla T\right]=h_T(T-T_{air})-h_m\frac{\left(p_{v\ eq}-p_{v\ air}\right)}{RT}h_{fg}M_w \quad , \tag{4}$$

where h_m is the mass transfer coefficient (m/s), h_T is the heat transfer

coefficient (W/(m^2·K)), $p_{v\ eq}$ is the equilibrium vapor pressure, $p_{v\ air}$ is the vapor air pressure of ambient air (Pa), **n** is the unit vector normal to the boundary, R is the universal gas constant (J/(mol·K)), T_{air} is the drying air temperature (K), M_w molar mass of water (g/mol) and h_{fg} is the latent heat of evaporation (J/kg). The equilibrium vapor pressure for each food material can be derived from the respective sorption isotherm. Therefore, the equilibrium vapor pressure for apple ($p_{v\ eq,apl}$) and potato ($p_{v\ eq,pot}$) are (Ratti et al., 1989),

$$p_{v\ \ eq\ ,apl} = p_{v\ \ sat}(T)\exp\Big(- 0.182M_{db}^{-0.696} + 0.232e^{-43.949M_{db}} M_{db}^{0.0411}\ \ln[p_{v\ \ sat}(T)]\Big)\ , \tag{5}$$

$$p_{v\ \ eq\ ,pot} = p_{v\ \ sat}(T)\exp\Big(- 0.0267M_{db}^{-1.656} + 0.0107e^{-1.287M_{db}} M_{db}^{1.513}\ \ln[p_{v\ \ sat}(T)]\Big). \tag{6}$$

where M_{db} is the moisture content dry bases (kg/kg dry bases), calculated using Equation A.2 and A.3 in Appendix A, and $p_{v\ sat}$ is the saturated vapor pressure, calculated by Equation A.1. A visual representation of equilibrium vapor pressure derived from Equation (5) and Equation (6) can be seen in Fig. 2 (a) and (b) respectively.

The last boundary condition is the symmetric condition applied at $r = 0$, defined as

$$\mathbf{n}\cdot\big[- D_{i,eff}\nabla C\big] = 0\ , \tag{7}$$

$$\mathbf{n}\cdot[-k\nabla T] = 0\ . \tag{8}$$

2.4. Food material properties

The thermophysical properties for each material are located within Table A.1 in Appendix A. These properties are a function of either moisture content, wet (M_{wb}) or dry (M_{db}) bases, and/or sample temperature. In summary, Apple had an initial moisture content of 6.8 kg/kg dry bases and an initial ICW content of 87.8% (Khan et al., 2018). Potato had an initial moisture content of 4.4 kg/kg dry bases and an initial ICW content of 81.3% (Khan et al., 2017).

2.5. Microscale mass conservation

To achieve the multiscale model, a microscale was established at each point in the macroscale representing the heterogeneous food structure. This assumption is valid when the scale parameter trends to zero, implying the heterogeneities vanish, leading to a homogeneous material (Welsh et al., 2021a; Auriault et al., 2010). This assumption is key when deriving a model via homogenization and is commonly referred to as the separation of scales (Auriault et al., 2010). The microscale considered two sub-domains, ICW denoted as ω_{ICW} and intercellular water [free water (FW)] denote as ω_{FW}, Fig. 1 (b). The macroscale mass transport, Equation (1), is coupled to the microscale mass transport equation defined as,

$$\frac{\partial c}{\partial t} + \frac{\partial}{\partial x}\left(-D\frac{\partial c}{\partial x}\right) + \frac{\partial}{\partial y}\left(-D\frac{\partial c}{\partial y}\right) = 0\ , \tag{9}$$

where c is the microscale concentration (mol/m^3) and D is the cellular diffusivity (m^2/s) equaling D_{ICW} if x,y ε ω_{ICW} and D_{FW} if x,y ε ω_{FW}.

2.5.1. Homogenized effective diffusivity

The 2D homogenized effective diffusivity is derived using Equation (9) and denoted by (Welsh et al., 2021a),

$$D_{H,eff} = \begin{bmatrix} \frac{1}{\omega}\int_{\omega} D(x,y)\left(\frac{\partial u_1}{\partial x} + 1\right) d\omega & \frac{1}{\omega}\int_{\omega} D(x,y)\frac{\partial u_2}{\partial x}\ d\omega \\ \frac{1}{\omega}\int_{\omega} D(x,y)\frac{\partial u_1}{\partial y}\ d\omega & \frac{1}{\omega}\int_{\omega} D(x,y)\left(\frac{\partial u_2}{\partial y} + 1\right) d\omega \end{bmatrix}, \tag{10}$$

where the area of the macroscale domain is ω, u_1 and u_2 are the corrective factors and the solution of the periodic cell problem,

$$\nabla\cdot\big(D\nabla\big(u_j + \mathbf{e_j}\big) = 0\ \ ,j = 1,2\ , \tag{11}$$

where

$$\mathbf{e_1} = \begin{bmatrix} 1 \\ 0 \end{bmatrix}\ ,\mathbf{e_2} = \begin{bmatrix} 0 \\ 1 \end{bmatrix}, \tag{12}$$

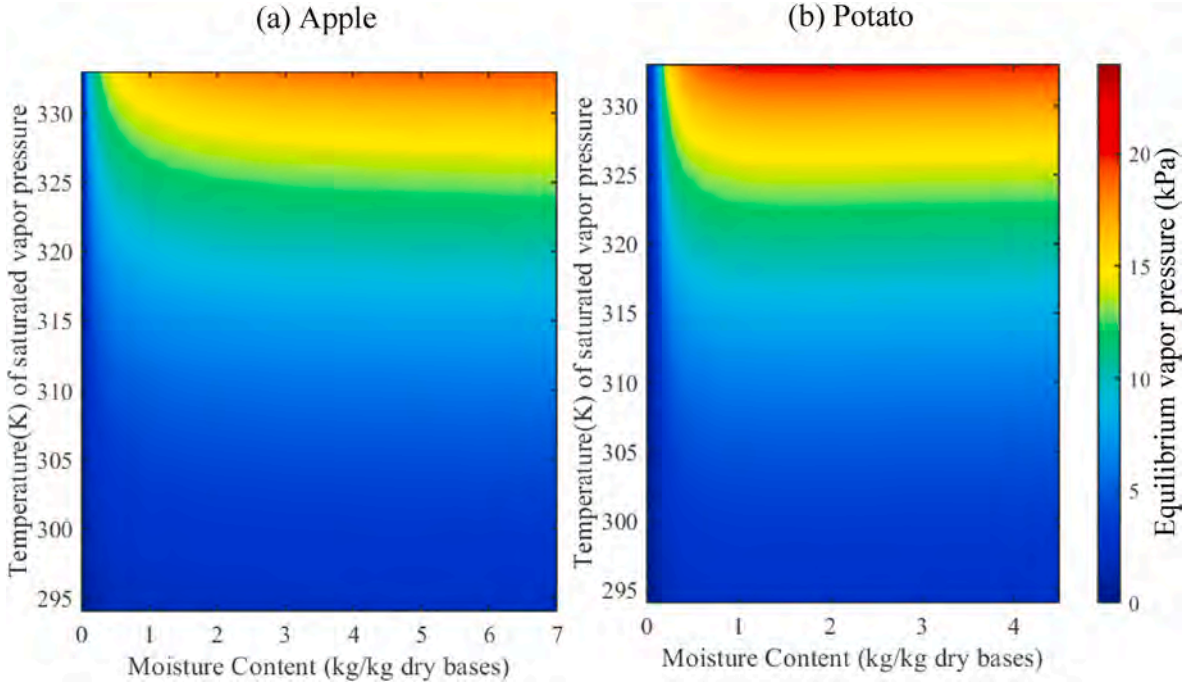

Fig. 2. Visual representation of the equilibrium vapor pressure (kPa) of (a) apple and (a) potato, Equation (5) and Equation (6) respectively.

$$u_1 = u_2 \; at \; \Gamma, \tag{13}$$

$$u_j \; is \; \omega - periodic \; , \tag{14}$$

$$\frac{1}{\omega}\int_A u_j d\omega = 0 \; . \tag{15}$$

The full derivation of the 2D homogenized diffusivity tensor, Equation (10), and the corrective factors, Equation (11), from the microscale mass conservation can be found in Appendix B. To calculate the homogenized diffusivity, the corrective factors are solved first and then the homogenized diffusivity is calculated. The corrective factors is unique only up to an additive constant (Auriault et al., 2010), requiring Equation (15), a zero mean constraint, to achieve a single unique solution. However, any of these unique solutions are suitable as the effective homogenized diffusivity only requires the gradient of u_j (Welsh et al., 2021a).

2.6. Cellular structure representation within the microscale domain

The cellular structure of apple contains some main components, namely the protoplast (composed of vacuole, tonoplast membrane and cytoplasm), the cell wall, the cell membrane and intercellular space (Prawiranto et al., 2018). These cellular components dynamically deform due to the various transport mechanisms occurring. Additionally, drying at different temperatures can cause different cellular deformation, adding complexities to representing the temporal heterogeneity of water (Khan et al., 2018). This work considers two sub-domains within the microscale, ICW denoted as ω_{ICW} and FW denote as ω_{FW}. This groups the effects of the protoplast, cell membrane and cell wall within the ICW domain. This lumping saves on computational cost but could have a negative effect on the accuracy of the model. The intercellular spaces were grouped and represented as a circle, Fig. 1 (b). This circle was assumed to be located at the center of the microscale domain, requiring minimal microstructural knowledge but forcing the homogenized diffusivity to be isotropic. The ratio between sub-domains within the microscale is the key factor to represent the materials heterogeneity (Welsh et al., 2021a). Additionally, to see the effects of grouping the intercellular spaces, a microscale domain investigation was conducted and can be found in Appendix C.

2.7. Cellular diffusivity properties for ICW and FW

To complete the homogenization, the diffusivity of each cellular subdomain is required. Welsh et al. (Welsh et al., 2021b) recently conducted a multiscale temporal investigation on the cellular diffusivity of apple tissue during drying. The work developed a function for the diffusivity of ICW incorporating cell rupturing within the property. The function is (Welsh et al., 2021b):

$$D_{ICW} = \exp\big[-110.32 + 0.55536T_s + 0.095148WC_{ICW} - 0.00090738T_s^2 - 0.0007235WC_{ICW}^2\big], \tag{16}$$

where T_s is the sample temperature (K) and WC_{ICW} is the intracellular water content (mass %). The function has only been validated for apple tissue, though its validity for other food material will be investigated within this work. The diffusivity of FW is (Pace, 1962):

$$D_{FW} = 2.26 \times 10^{-5}\left[\frac{T}{273.15}\right]^{1.81} . \tag{17}$$

2.8. Evolution of intracellular water-rupturing threshold

In order to use Equation (16) ICW and its evolution during drying had to be considered within the model. ICW has the ability to transport three main ways: cell to cell, cell to pore or through a cell membrane rupture (Khan et al., 2018). Commonly only cell to cell and cell to pore transport is considered within theoretical models, even though cell rupturing can significantly influence the transport process, associated deformation and the quality of a dried product (Khan et al., 2018). Deformation and cell collapse can be caused indirectly by gradients of temperature, difference in vapor pressure, or in osmotic pressure between the product and the surrounding environment (Prothon et al., 2003). The ICW diffusivity function [Equation (16)] incorporates all three transport mechanisms, therefore, cell rupturing must be incorporated within the evolution of ICW. The model must be able to recognize if, when and the rate at which cell rupturing has occurred. It is well established cell rupturing occurs due to a loss in turgor pressure and is a local mechanism. Additionally, turgor pressure is linked and has an impact on the sorption isotherm of the protoplast within the material (Prawiranto et al., 2018). Turgor pressure (Pa) is

$$\psi_p = \psi_c - \psi_s, \tag{18}$$

where Ψ_c is the osmotic potential (Pa) and Ψ_s is the water potential (Pa) at the cytoplasma side of the cell membrane. This approach has been utilized within dehydration models in relation to the water activity, however cell rupturing was not incorporated. Within the field of food drying, cell rupturing is commonly described in association with temperature and is quite common at higher temperatures. However, understanding and quantifying cell rupturing during drying is extremely complex and involves sophisticated experimentation. As a result, limited studies have been conducted into cell rupturing during drying of plant-based food materials. Using a bioelectric impedance method, it was uncovered that cell walls begin to rupture once the sample has reached a temperature of about 50 °C (Halder et al., 2011). To further advance this understanding, the current authors attempted to investigate the cell rupturing mechanism using Nuclear Magnetic Resonance (NMR). Based on the NMR T_2 relaxometry, the water status inside a material can be determined. However, although NMR T_2 signal intensity provides the local information, it cannot exactly quantify the cell to cell or individual cell water status within the material. Therefore, it provides the local scale information as a global average. Based on this principle, cell rupturing phenomena can be predicted. It was argued that once the products surface reaches 50 °C during drying, the cell adjacent to the surface lose their rigidity and tend to become droopy (near rupturing limit). The cells within this region los turgor pressure and tend to fail due to the imposed thermal stress due to the continuous penetration of heat energy (Khan et al., 2018). Once the cells adjacent to the samples surface rupture, the cellular water migrates from intracellular space to intercellular spaces and becomes FW, therefore increasing the proportion of FW as compared to ICW in the sample. As drying continues to progress, the continuous evaporation causes the new FW to be easily transported, resulting in the FW content decreasing in the sample and the proportion of ICW increasing in respect to the total water composition of the sample. This continuous process creates a fluctuating ICW trend when considering the total water proportion within the sample. This has been demonstrated for various food materials (low and highly porous) (Khan et al., 2018; Khan et al., 2017).

With this in mind, the current work utilizes the macroscale equilibrium vapor pressure to determine if and when cell rupturing occurs. An investigation will be conducted to develop a theoretical equilibrium vapor pressure threshold utilizing the average of the domain, following a similar methodology of how NMR provides local water information grouped as a global average. The equilibrium vapor pressure is a product dependent relationship constructed through the material sorption isotherm (Ratti et al., 1989). The property is moisture and temperature dependent and as the material dries, $p_{v\,eq}$ at the surface experiences an initial increase, before decreasing (pressure drop). As the material heats up a large pressure difference can be generated within the material depending on the drying temperature. This phenomenon will be exploited to characterize which transport mechanisms are occurring

within the material. The investigation will consider convective drying at 50 °C, utilizing the known cell membrane temperature limit to uncover the maximum equilibrium vapor pressure at this temperature. This maximum will become the theoretical threshold. A visual representation of the threshold can be seen in Fig. 3. When the threshold is not reached, cell rupturing will not occur and WC_{ICW} will remain constant at its initial value, Fig. 3 (a). When $p_{v\ eq}$ exceeds the threshold, cell rupturing will occur and WC_{ICW} will linearly decrease, Fig. 3 (b). This corresponds to the assumption within (Welsh et al., 2021b). The rate at which WC_{ICW} decrease is formulated from Khan et al. (2018) and Khan et al. (2017) for apple and potato respectively. This results in ICW content functions of $-0.0033 \times t + 87.8$ for apple and $-0.003 \times t + 81.3$ for potato when cell rupturing occurred. The locality of cell rupturing was unable to be captured by this approach.

2.8.1. Remaining properties

The remaining input parameters are summarized in Table A.2. Due to the perpendicular airflow within the dryer, the heat transfer coefficient was calculated as 13.2 (W/(m^2·K)) utilizing a computational fluid dynamics model previously published by the authors (Imran et al., 2020).

2.9. Mass transfer coefficient

The mass transfer coefficient is also a condition-dependent parameter. It is strongly influenced by the airflow distribution and deformation the product experiences (Defraeye and Radu, 2018). Imran et al. (2020) investigated spatial dependent heat and mass transfer coefficients demonstrating their influence on the drying kinetics. The work concluded a larger overpredict can occur if the spatial distribution of airflow is not considered. Therefore, to minimize the mass transfer coefficient influence on the results it will be solved through an inverse problem. This allowed the study to focus on investigating the generalized diffusivity. For the inverse problem, the mass transfer coefficient (h_m) is unknown and predicted based on the minimization between the simulated and experimental moisture drying curves. A Levenberg-Marquardt optimization algorithm coupled with the finite element method was applied with the objective functions as

$$OF(h_m) = \int \left[\overline{M}_{db,\exp}(t) - \overline{M}_{db,num}(t, h_m)\right]^2 dt, \tag{19}$$

where $\overline{M}_{db,\exp}$ is the average dry bases moisture content from the experimental investigation and $\overline{M}_{db,num}$ is the average dry bases moisture content from the simulation.

2.10. Computational strategy

The modeling procedure is shown in Fig. 4. The upscaled effective diffusivity was solved in MATLAB 2018a coupled with Gmsh to construct the microscale domains. Once $D_{H,eff}$ was solved, the cell rupturing investigation was conducted. Both the cell rupturing investigation and the macroscale heat and mass transport model were solved in COMSOL Multiphysics 5.3a. Lastly, a sensitivity investigation was conducted on some key parameters with uncertainty.

3. Experimental investigation

Two different food materials are investigated within this work, Granny Smith apples and Brushed potatoes. They were purchased from a local supermarket at commercial maturity. The samples were prepared based on the standard sample preparation procedure (Asabe and Home). Each product was washed and cut into cylindrical slices (mesocarp of pulp portions) using a fruit sample preparation tool [a stainless-steel Cork Borer (JH-1225)]. The initial dimensions of the samples were 30 mm in length and 18 mm in diameter. Typically, convective food drying is conducted at temperatures between 40 and 80 °C. Therefore, the drying experiments were performed at mean temperatures of 47 °C and 64 °C with an air velocity of 1 m/s. The velocity was measured inside the drying chamber with a handheld anemometer just in front and above the leading edge of the sample. These temperatures were selected as examples as two different types of cellular deformation (minimal cellular deformation and significant deformation). The driers inlet and outlet were perpendicular to one another creating uneven velocity distribution. Two sets of experiment data were required to validate the model: the average moisture content and average surface temperature of the sample. To record the moisture content, each sample was weighed individually in regular intervals throughout the drying process, every 10 min for the first hour then every 30 min till completion. This was done utilizing a digital electronic balance with a capacity of 50 g and an accuracy of ±0.001 g. The measurements were completed within 10 s during the drying process. To record the sample surface temperature, a thermal image camera was utilized (FLIR-E6390). The experimental procedure was replicated three times. Therefore, a total of 12 samples were dried, 6 apple samples and 6 potato samples.

4. Results

The results are presented in four main parts: the upscaled effective diffusivity, drying at low temperatures (47 °C), drying at medium temperatures (64 °C) and a sensitivity investigation. Drying at low temperatures results is no cell rupturing whereas significant cell rupturing

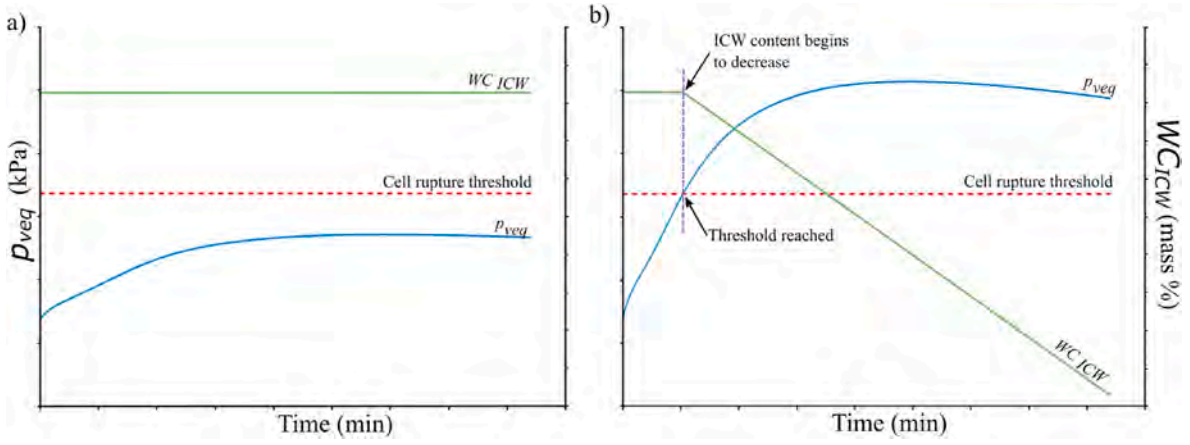

Fig. 3. Visual representation of proposed theoretical cell rupturing threshold, a) threshold is not reached and cell rupturing does not occur, b) threshold is reached and cell rupturing occurs.

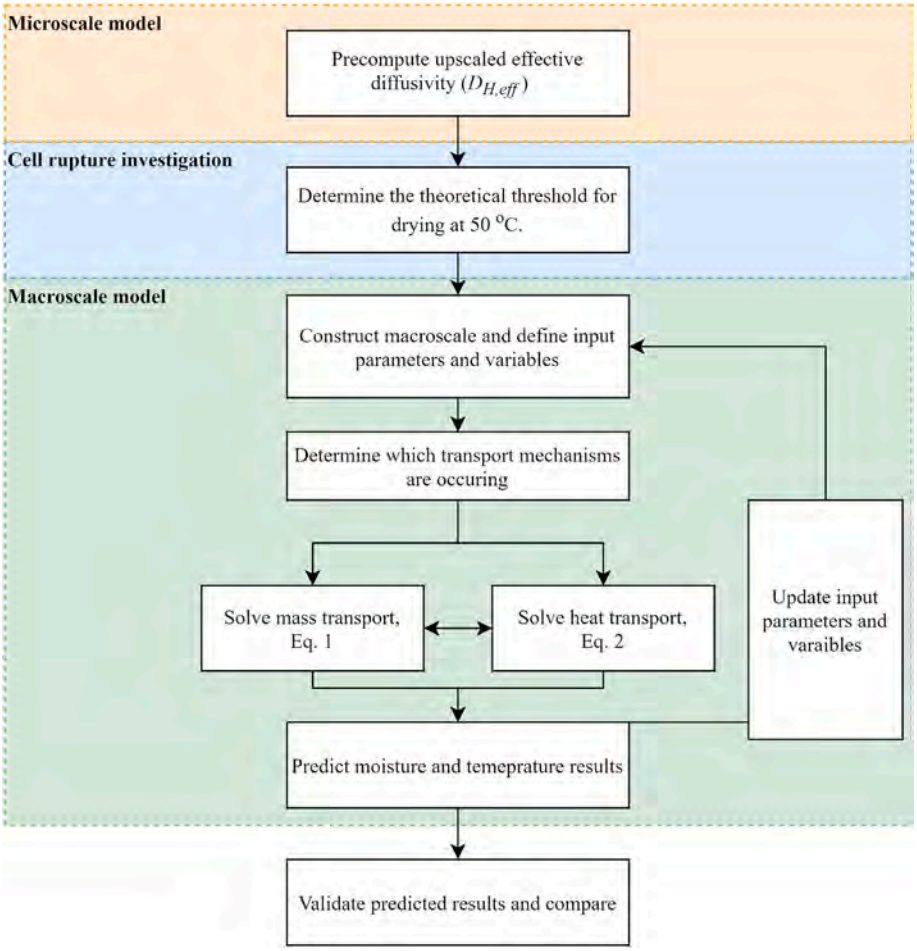

Fig. 4. Computational methodology.

occurs when drying at medium temperatures. This allows the predictive capabilities of the generalized diffusivity to be investigated in depth. The equilibrium vapor pressure investigation is presented within section 4.3. All error bars displayed within the results show plus-minus one standard deviation of the mean experimental data.

4.1. Upscaled effective diffusivity

Homogenization was performed for all combinations of sample temperature (T_s) and intracellular water content (WC_{ICW}) to construct the generalized effective diffusivity function. This created the following function,

$$D_{H,eff} = \exp\left[-106.6 + 0.5548T_s + 0.029502WC_{ICW} - 0.00090648T_s^2 - 0.00041019WC_{ICW}^2 \right]. \quad (20)$$

A visual representation of the upscaled effective diffusivity can be seen in Fig. 5. Most food materials have an initial ICW content between 76 and 92% (represented by the red boundaries in Fig. 5). Within this region, there is a gradient in both ICW content and temperature. As the ICW content decreases, the effective diffusivity increases. This is because there is a higher percentage of FW with the sample and as FW is easily transported. As temperature increases within this region, the diffusivity initially increases before tapering off at higher temperatures. However, the effective diffusivity does remain fairly constant if cell rupturing doesn't occur. Once cell rupturing occurs (region below the bottom red boundary), the diffusivity significantly increases. When there is minimal ICW left in the material the diffusivity decreases.

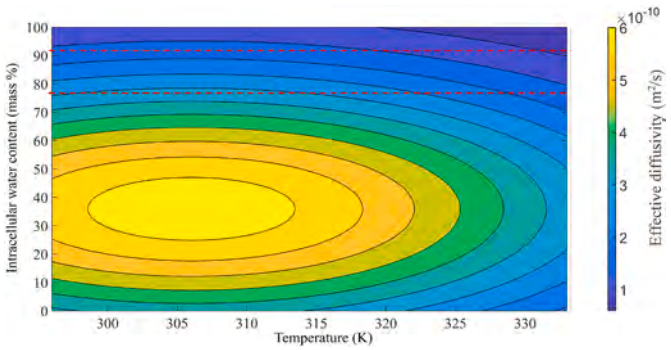

Fig. 5. Visual representation of the effective diffusivity (m^2/s) function.

4.2. Drying at low temperatures - no cell rupturing occurs

4.2.1. Mass transfer coefficient

The mass transfer coefficient (h_m) was solved through an inverse problem for drying apple at low temperatures. This approach resulted in a lower than expected average mass transfer coefficient of 0.00381 m/s. This value was used for the remainder of the study. During food drying, the mass transfer coefficient depends on the velocity field (spatially dependent) and macroscale deformation (temporal dependent). Literature demonstrates models tend to overpredict experimental data when not considering a spatially dependent mass transfer coefficient (h_m) (Imran et al., 2020) and can underpredict experimental data when considering a spatially dependent h_m without macroscale deformation

(Defraeye and Radu, 2018). Deformation is interconnected and a biproduct of the complex heat and mass transfer which occurs. Deformation changes the size of the sample influencing the mass transfer coefficients in addition to the diffusivity, and thus affects the rate at which moisture evolves. When deformation is not considered, the mass transfer coefficient is over-estimated and the rate at which moisture evolves with time is over-predicted. The presented model does not consider a varying velocity field or the macroscale deformation, rather compensating for their effects through the inverse calculation of the mass transfer coefficient.

4.2.2. Drying kinetics

The presented multiscale model accurately predicts drying at lower temperatures achieving a low mean relative error (MRE) of 1.52% for apple and 3.18% for potato, Fig. 6. The generalized diffusivity was successful in distinguishing between the two materials through considering their ICW content. Apples and potatoes have different initial ICW contents, 87.8% and 81.3% respectively. This resulted in a difference in their effective diffusivities, Fig. 7. These values can be compared to literature cautiously, due to the condition-dependent nature of previously published diffusivity data. The magnitudes of the generalized diffusivity can be compared to 1.594×10^{-10} m^2/s for Granny smith apples at 40 °C (Simpson et al., 2015) and $3.6 \times 10^{-10} - 4.3 \times 10^{-10}$ m^2/s for potato at 40 °C (Hassini et al., 2007).

4.2.3. Temperature profile

The presented model accurately predicts the average temperature profile when drying at lower temperatures, Fig. 8. The model achieved low MREs of 0.46% for apple and 0.65% for potato. However, the model does significant overpredict the temperature profile in the early stages of drying. This also caused a sharp initial increase in diffusivity, Fig. 6. This overprediction is consistent with models in literature which consider a constant/average heat transfer coefficient (Welsh et al., 2021a; Imran et al., 2020; Defraeye and Radu, 2018). To improve the temperature profile, the heat transfer coefficient could be considered in terms of a velocity field (spatially dependent) (Imran et al., 2020) and/or in terms of the deforming sample (Mahiuddin et al., 2018). However, this would increase the computational cost of the model. Additionally, applying multiscale modeling to the thermal conductivity of the material could help further minimize this overprediction.

4.2.4. Drying at medium temperatures - significant cell rupturing occurs

Before the generalized diffusivity could be applied to drying at medium temperatures, the equilibrium vapor pressure threshold investigation was conducted.

4.2.5. Rupture threshold development

The results of the equilibrium vapor pressure threshold investigation

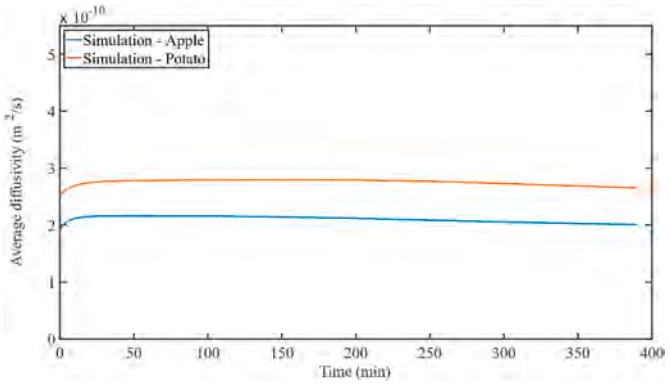

Fig. 7. Average diffusivity (m^2/s) for drying at 47 °C.

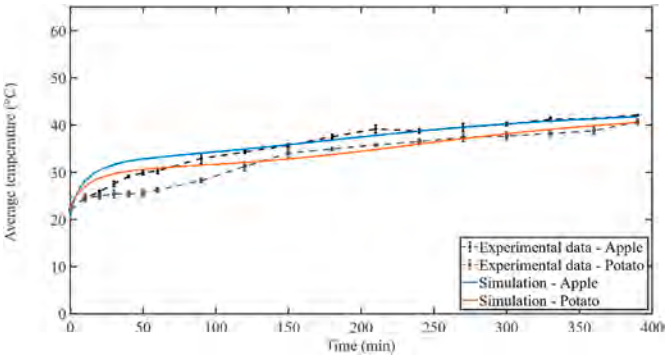

Fig. 8. Average Temperature (°C) for drying at 47 °C. Error bars represent plus-minus one standard deviation of the triplicate experimental data.

can be seen in Fig. 9. The investigation considered the upscaled diffusivity, Equation (20), while drying at 50 °C. Additionally, it was assumed cell rupturing had not occurred, therefore WC_{ICW} remained constant at their initial percentages. This resulted in a unique threshold for each food material, 7080 Pa for apple and 8004 Pa for potato. The spatial distribution of each material at their associated threshold can also be seen in Fig. 9 (a) and Fig. 9 (b) for apple and potato respectively.

4.2.6. Drying kinetics

The presented model accurately predicts the drying kinetics at medium temperatures, Fig. 10. The model achieved MREs of 4.8% for apple and 7.8% for potato, slightly worse MREs than drying at lower temperatures. The greatest deviation between the experiment data and simulations can be seen in the latter stages of drying, especially for

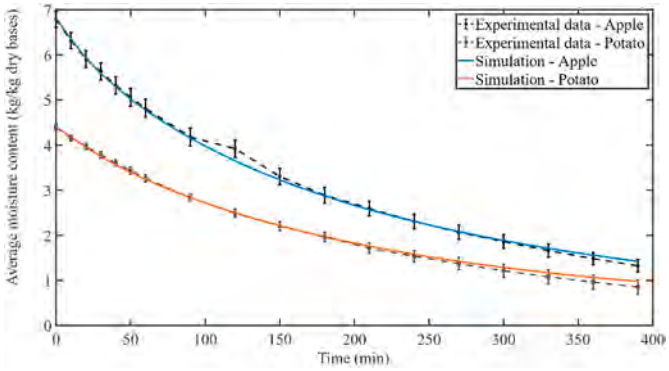

Fig. 6. Average moisture content (kg/kg dry bases) for drying at 47 °C. Error bars represent plus-minus one standard deviation of the triplicate experimental data.

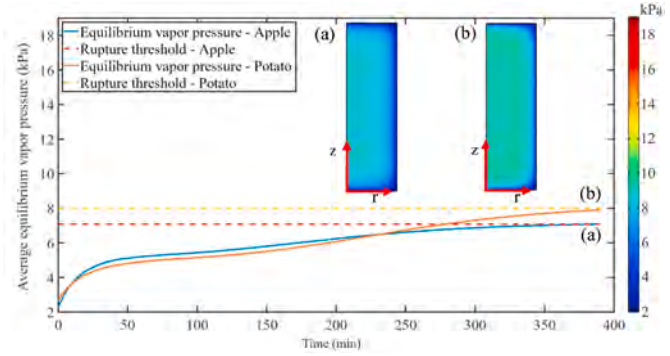

Fig. 9. Rupturing threshold investigation using the average equilibrium vapor pressure (kPa), (a) spatial distribution of apple at threshold and (b) spatial distribution of potato at threshold.

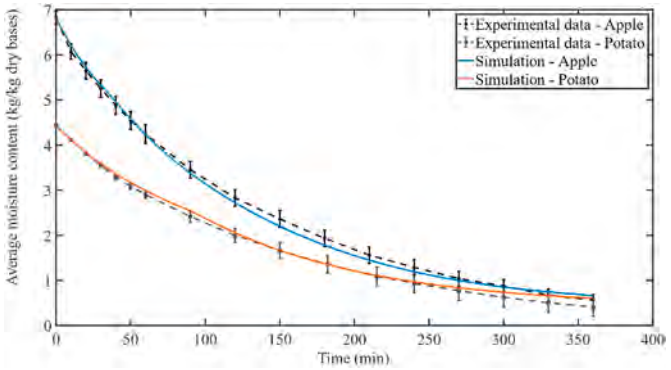

Fig. 10. Average moisture content (kg/kg dry bases) for drying at 64 °C. Error bars represent plus-minus one standard deviation of the triplicate experimental data.

potato. Though, the model remains within the error bars. The resulting effective diffusivities can be seen in Fig. 11. Once the rupture threshold is reached, the diffusivity experiences a sudden jump. This is a limitation of the assumed trend of ICW when cell rupturing occurs; trend is precomputed rather than computed on the fly. The unique rupture thresholds cause cell rupturing to commence at different points in time for both materials, mimicking the real world (Khan et al., 2018; Khan et al., 2017). The effective diffusivity results can be compared to 0.713 $\times 10^{-11}$ - 7.66 $\times 10^{-10}$ m^2/s for Red Delicious apples at a temperature range of 35–55 °C (Beigi, 2016) and 5.42 $\times 10^{-10}$ – 1.92 $\times 10^{-9}$ m^2/s for drying potato at 40–70 °C (Hassini et al., 2007).

4.2.7. Temperature profile

The presented model predicted the average temperature reasonably well achieving a low MRE of 0.89% for apple and 0.67% for potato, Fig. 12. These MREs are similar to drying at lower temperatures. The same overprediction exists in the early stages of drying. Looking closely at Fig. 12, potato doesn't experience a smooth transition when the rupture threshold is reached (at 92 min), but stabilizes as drying continues. Apple on the other hand does experience a smooth transition once the threshold is reached.

4.2.8. Equilibrium vapor pressure when drying at medium temperatures

The average equilibrium vapor pressure in relation to the ICW content can be seen in Figs. 13 and 14 for apple and potato respectively. When the rupture threshold is reached, minimal pressure gradient exists within the sample. The distribution is very similar to the distribution uncovered within the threshold development. This can be seen when comparing Fig. 9 (a) and (b) to Figs. 13 (a) and Fig. 14 (a). Once the threshold is reached, a significant pressure gradient develops. This trend exists for both materials.

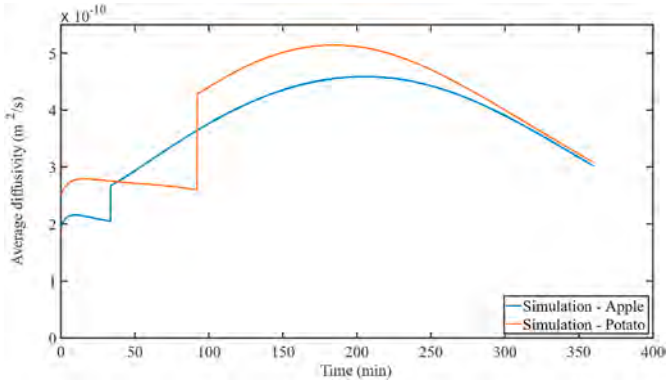

Fig. 11. Average diffusivity (m^2/s) for drying at 64 °C.

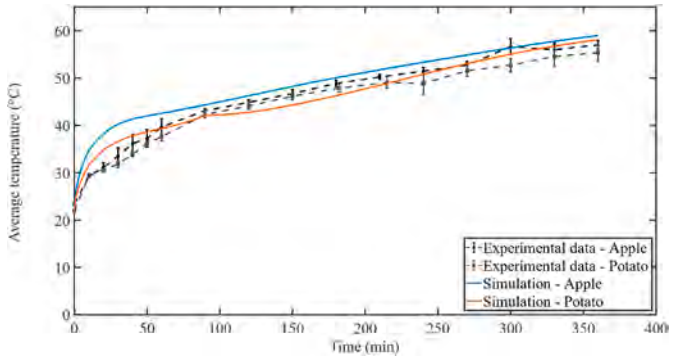

Fig. 12. Average temperature (°C) for drying at 64 °C. Error bars represent plus-minus one standard deviation of the triplicate experimental data.

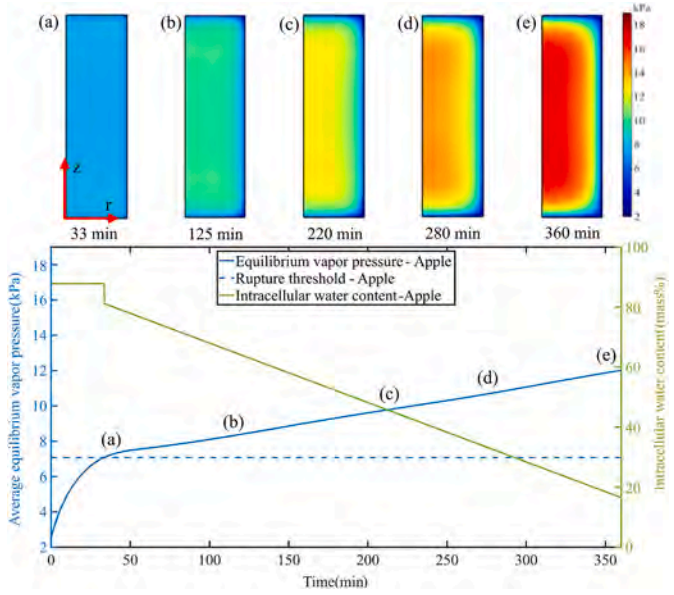

Fig. 13. The average equilibrium vapor pressure (kPa) and ICW content (mass %) of apple drying at 64 °C. Spatial distribution of the equilibrium vapor pressure at (a) 33 min (when threshold is reached), (b) 125 min, (c) 220 min, (d) 280 min and (e) 360 min.

The ICW content with respect to time can be seen for each material in Figs. 13 and 14. Each material remains at its initial percentage until the threshold is reached. Once the rupture threshold is reached the ICW content linearly decreases. The rate at which ICW linearly decreases was precomputed based on the initial and final ICW percentages within published literature (Khan et al., 2018; Khan et al., 2017). This precomputation creates the sharp drop in ICW content when the threshold is reached for each material. Potato reaches its threshold later in drying therefore the drop is greater, causing the uneven transition discussed within the temperature profile (Fig. 12).

4.3. Sensitivity investigation

The constructed multiscale model requires a large number of input parameters, Table A.1 and Table A.2. Some of these key parameters contain uncertainty or variability due to their availability in literature and the nature of fruits and vegetables. Therefore, it is important to conduct a sensitivity investigation to have greater confidence in the simulated model. For example, the density of apple tissue can vary from the inner and outer parenchyma by about 12%. To evaluate the sensitivity of the predicted model, the material density and the heat transfer coefficient were investigated in relation to the average moisture content

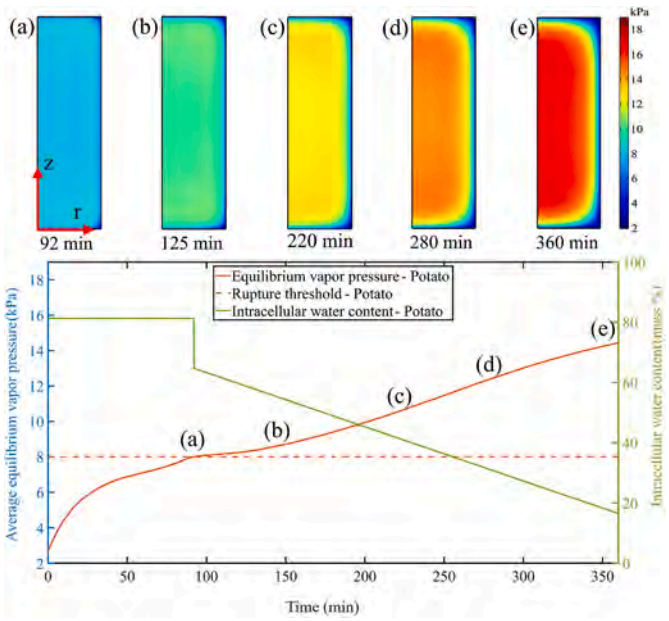

Fig. 14. The average equilibrium vapor pressure (kPa) and ICW content (mass %) of potato drying at 64 °C. Spatial distribution of the equilibrium vapor pressure at (a) 92 min (when threshold is reached), (b) 125 min, (c) 220 min, (d) 280 min and (e) 360 min.

(kg/kg dry bases) and average temperature (°C) by varying the utilized values by ± 10% for drying at low temperatures.

The presented model's sensitivity to density can be seen in Fig. 15. The average moisture content is not sensitivity to the change in density, Fig. 15 (a). However, the changes in density does influence the temperature profile in the later stages of drying. For both materials, plus 10% underpredicts the average temperature, whereas minus 10% causes a small overprediction, Fig. 15 (b). The change in density did not improve the model's ability to predict the temperature profile in the early stages of drying.

The presented model's sensitivity to the heat transfer coefficient can be seen in Fig. 16. The moisture content was not sensitivity to the varying heat transfer coefficient, Fig. 16 (a), however as expected, the temperature profile was influenced by the change in heat transfer coefficient. For both materials, plus 10% caused a very small overprediction in the temperature profile, whereas minus 10% caused a substantial underprediction, Fig. 16 (b). Therefore, underpredicting the heat transfer coefficient has a larger influence on the presented model.

5. Discussion

The generalized diffusivity successfully describes drying at low and medium temperatures for both materials. The effective diffusivity function was able to distinguish the materials through their ICW content rather than their porosity. The generalized diffusivity is in terms of temperature and ICW content, allowing the property to be applicable for multiple materials (apple and potato) drying at multiple temperatures (with different microstructural deformation). The theoretical cell rupturing threshold allowed the property to appropriately adapt to the different drying conditions. At low temperatures the threshold is not reached, and the effective diffusivity remains fairly constant, Fig. 7. This suggests an average diffusion coefficient is sufficient when drying at lower temperatures. Defraeye and Verboven (2017) also concluded that a constant diffusivity coefficient is sufficient for engineering problems drying at low temperatures (20 °C). At medium temperatures the threshold is reached, causing the effective diffusivity to spike and peak in the middle stages of drying, Fig. 11. This is somewhat contradictory to published literature where generally the effectivity diffusivity gradually decreases with moisture (Dadmohammadi and Datta, 2019; Hassini et al., 2007). Though these studies do not consider cell rupturing. It is well established FW is effortlessly transported during drying (Welsh et al., 2018). Therefore, if we assume once a cell is ruptured the ICW water rushes out of the cell and becomes FW, logically there should be a spike/large increase in the effective diffusivity of the material. Toward the latter stages of drying the effective diffusivity drops off, matching the published trends in literature, Fig. 11. Though it is unclear if the magnitude of the drop is correct. The presented model does begin to deviate in the latter stages of drying. In fact, the model deviates in the latter stages for both materials at both drying temperatures, most predominate is potato drying at 64 °C. The model simplifies some aspects of food material such as considering the material as single phase, no macroscale deformation and considering an average mass transfer

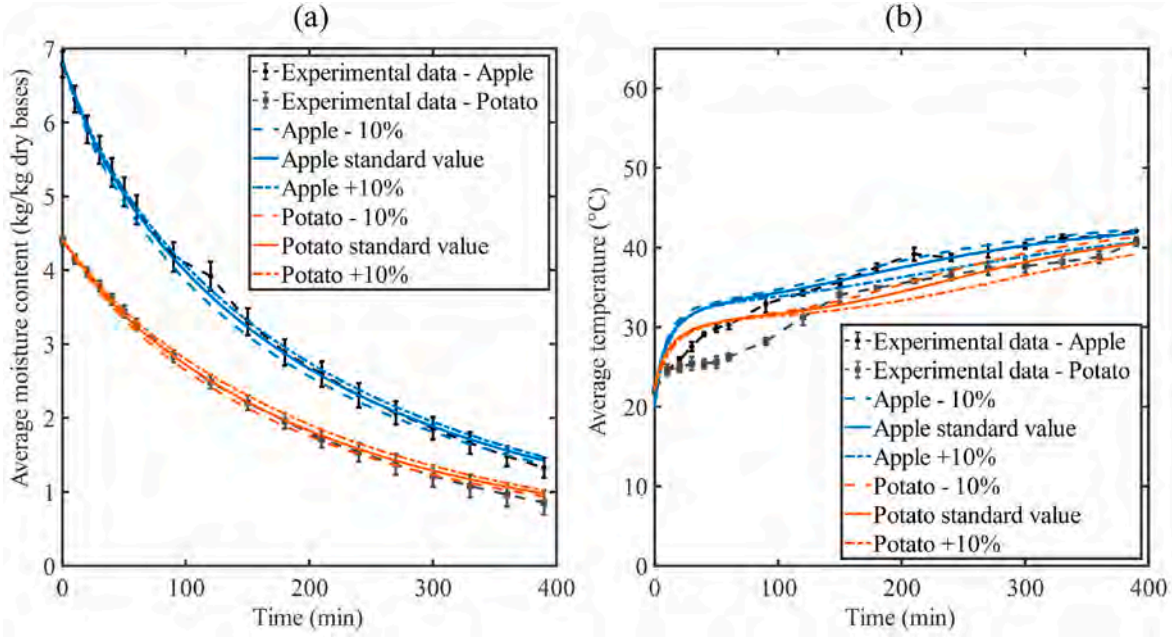

Fig. 15. Sensitivity investigation for the material density ±10%, a) average moisture content (kg/kg dry bases), b) average temperature (°C).

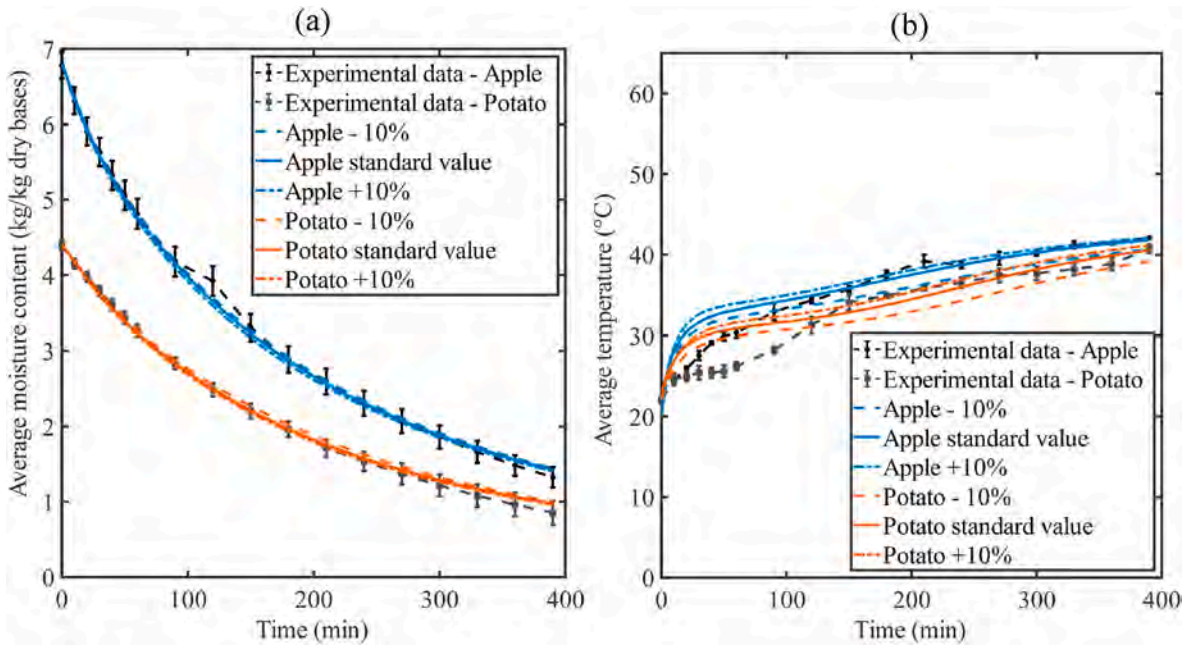

Fig. 16. Sensitivity investigation for the heat transfer coefficient ±10%, a) average moisture content (kg/kg dry bases), b) average temperature (°C).

coefficient. This was done to keep a reasonable computational cost and to focus on the generalized diffusivity. Vapor transport can play a large role in the final stages of drying when the material is at low moisture contents. Some consideration of the macroscale deformation, a multiphase material and/or transfer coefficients which are spatially dependent and/or influenced by deformation will improve the model's prediction in the latter stages.

There were a couple of key assumptions made in order to achieve the novel generalized property. These were centrally focused around the ICW and its trend during drying. The first major assumption was to assume the ICW content remains constant at its initial percentage when cell rupturing does not occur. When drying at lower temperatures (where cell rupturing does not occur) the average ICW content over the drying time is slightly below its initial percentage (roughly 5% below, inferred from (Welsh et al., 2021a)). This is due to the evolution of the material, microscale deformation and porosity. Considering this marginal difference would require comprehensive knowledge of the microstructural evolution (extensive experimental investigation) and increase the computational cost. Therefore, the assumption was made to keep the ICW content constant at its initial percentage. The rate at which ICW linearly decreased when cell rupturing occurs was the second key assumption. The rate was deduced from published literature (Khan et al., 2018; Khan et al., 2017) and considered in terms of drying time. This is not ideal and is a limitation of the presented model. Additionally, this approach creates a discontinuity for ICW, which can be seen in Figs. 13 and 14. To fully explain the discontinuity's effect upon the model, a further investigation was conducted and presented in Appendix D. More work is required to develop an improved function describing the trend of ICW content once the cell rupturing threshold is reached. Recent advancements in experimental investigating techniques will aid in developing these functions (Khan et al., 2018). Additionally, although the theoretical cell rupturing threshold was able to predict if and when cell rupturing occurs, it was unable to consider the locality of cell rupturing as it evaluated the average of the domain. Ideally, the rupture threshold would predict the location in addition to if and when the rupture occurred. However, this would require a concurrent multiscale model, where the microscale is fully coupled to the macroscale, solved simultaneously and information is fed between scales at each time step (Welsh et al., 2018). Additionally, to fully capture the locality of cell rupturing, the microscale would need to model or incorporate the turgor pressure of cells. It should be noted, such an approach would be extremely computationally expensive. The theoretical threshold approach is simple, yet an effective method of determining which transport mechanisms are occurring and will serve as a steppingstone to fully integrate cell rupturing into physics-based food drying models.

6. Conclusion

The generalized diffusivity successfully described drying at low and medium temperatures for both materials (apple and potato). A novel theoretical equilibrium vapor pressure threshold was introduced, allowing the model the recognize if and when cell rupturing had occurred. This resulted in unique rupture thresholds for each material. Being able to recognize if cell rupturing has occurred greatly improved the predictive capabilities of the diffusivity. Additionally, this will allow future researchers to conduct in depth optimization investigations. The generalized property resulted in effective diffusivities of 1.94×10^{-10}-4.59×10^{-10} m^2/s for apple and 2.51×10^{-10}-5.14×10^{-10} m^2/s for potato. The presented model only moderately predicted the experimental temperature profile. The model could be refined by introducing more general heat and mass transfer coefficients that depend on position and time as a result of material deformation. However, this will increase the computational cost of the mathematical model. The generalized diffusivity will aid in mathematical food drying models reaching their full potential.

Author contributions

Zachary G. Welsh: Concept development, modelling, analysis, manuscript drafting, reviewing and editing. **Matthew J. Simpson**: Mathematical modelling and reviewing & editing. **Md Imran H. Khan**: Experiments, analysis, reviewing & editing. **M. A. Karim**: Project leader, concept development, reviewing & editing.

Declaration of competing interest

The authors declare that they have no known competing financial interests or personal relationships that could have appeared to influence the work reported in this paper.

Data availability

Data will be made available on request.

Acknowledgements

This study was funded by the Department of Education and Training (AUS) through a Research Training Program (Stipend) Domestic (RTP) scholarship and the ARC Grants LP200100493 and DP220103668.

Appendix E. Supplementary data

Supplementary data to this article can be found online at https://doi.org/10.1016/j.jfoodeng.2022.111309.

References

Adrover, A., Brasiello, A., Ponso, G., 2019/03/01/2019. A moving boundary model for food isothermal drying and shrinkage: general setting. J. Food Eng. 244, 178–191.
J. Asabe and A. Home, "American society of agricultural and biological engineers".
Auriault, J.-L., Boutin, C., Geindreau, C., 2010. Homogenization of Coupled Phenomena in Heterogenous Media, vol. 149. John Wiley & Sons.
Beigi, M., 2016/10/01 2016. Influence of drying air parameters on mass transfer characteristics of apple slices. Heat Mass Tran. 52, 2213–2221.
Dadmohammadi, Y., Datta, A.K., 2019. Prediction of Effective Moisture Diffusivity in Plant Tissue Food Materials over Extended Moisture Range. Drying Technology, pp. 1–15.
Defraeye, T., 2014. Advanced computational modelling for drying processes – a review. Appl. Energy 131, 323–344.
Defraeye, T., Radu, A., 2018. Insights in convective drying of fruit by coupled modeling of fruit drying, deformation, quality evolution and convective exchange with the airflow. Appl. Therm. Eng. 129, 1026–1038.
Defraeye, T., Verboven, P., 2017/01/01/2017. Convective drying of fruit: role and impact of moisture transport properties in modelling. J. Food Eng. 193, 95–107.
Halder, A., Datta, A.K., Spanswick, R.M., 2011. Water transport in cellular tissues during thermal processing. AIChE J. 57, 2574–2588.
Hassini, L., Azzouz, S., Peczalski, R., Belghith, A., 2007/03/01/2007. Estimation of potato moisture diffusivity from convective drying kinetics with correction for shrinkage. J. Food Eng. 79, 47–56.
Imran, M., Khan, H., Welsh, Z., Gu, Y., Karim, M.A., Bhandari, B., 2020/06/01/2020. Modelling of simultaneous heat and mass transfer considering the spatial distribution of air velocity during intermittent microwave convective drying. Int. J. Heat Mass Tran. 153, 119668.
Khan, M.I.H., Wellard, R.M., Nagy, S.A., Joardder, M.U.H., Karim, M.A., 2017/07/01/2017. Experimental investigation of bound and free water transport process during drying of hygroscopic food material. Int. J. Therm. Sci. 117, 266–273.
Khan, M.I.H., Nagy, S.A., Karim, M.A., 2018/03/01/2018. Transport of cellular water during drying: an understanding of cell rupturing mechanism in apple tissue. Food Res. Int. 105, 772–781.
Khan, M.I.H., Farrell, T., Nagy, S.A., Karim, M.A., 2018/10/12 2018. Fundamental understanding of cellular water transport process in bio-food material during drying. Sci. Rep. 8, 15191.
Mahiuddin, M., Khan, M.I.H., Kumar, C., Rahman, M.M., Karim, M.A., 2018. Shrinkage of food materials during drying: current status and challenges. Compr. Rev. Food Sci. Food Saf. 17 (5), 1113–1126.
Pace, E.L., 1962/08/01 1962. Scientific foundations of vacuum technique (Dushman, Saul). J. Chem. Educ. 39, A606.
Perré, P., 2007. Multiscale aspects of heat and mass transfer during drying. Transport Porous Media 66, 59–76.
Prawiranto, K., Defraeye, T., Derome, D., Verboven, P., Nicolai, B., Carmeliet, J., 2018/12/01/2018. New insights into the apple fruit dehydration process at the cellular scale by 3D continuum modeling. J. Food Eng. 239, 52–63.
Prawiranto, K., Carmeliet, J., Defraeye, T., 2020. Identifying in silico how microstructural changes in cellular fruit affect the drying kinetics. Soft Matter 16, 9929–9945.
Prothon, F., Ahrné, L., Sjöholm, I., 2003/07/01 2003. Mechanisms and prevention of plant tissue collapse during dehydration: a critical review. Crit. Rev. Food Sci. Nutr. 43, 447–479.
Qiu, S., Xu, S., Rao, B., Mujumdar, A.S., Xu, P., 2022/12/01/2022. A multi-scale model for impingement drying of porous slab. J. Food Eng. 335, 111194.
Ratti, C., Crapiste, G., Rotstein, E., 1989. A new water sorption equilibrium expression for solid foods based on thermodynamic considerations. J. Food Sci. 54, 738–742.
Simpson, R., Ramírez, C., Birchmeier, V., Almonacid, A., Moreno, J., Nuñez, H., et al., 2015/12/01/2015. Diffusion mechanisms during the osmotic dehydration of Granny Smith apples subjected to a moderate electric field. J. Food Eng. 166, 204–211.
Tzempelikos, D.A., Mitrakos, D., Vouros, A.P., Bardakas, A.V., Filios, A.E., Margaris, D.P., 2015. Numerical modeling of heat and mass transfer during convective drying of cylindrical quince slices. J. Food Eng. 156, 10–21.
Welsh, Z., Simpson, M.J., Khan, M.I.H., Karim, M., 2018. Multiscale modeling for food drying: state of the art. Compr. Rev. Food Sci. Food Saf. 17, 1293–1308.
Welsh, Z.G., Khan, M.I.H., Karim, M., 2021a. Multiscale modeling for food drying: a homogenized diffusion approach. J. Food Eng. 292, 110252.
Welsh, Z.G., Simpson, M.J., Khan, M.I.H., Karim, A., 2021b. A multiscale approach to estimate the cellular diffusivity during food drying. Biosyst. Eng. 212, 273–289.